Check for updates

Spatially heterogeneous dynamics of cells in a growing tumor spheroid: comparison between theory and experiments

Sumit Sinha, [a] Abdul N. Malmi-Kakkada,[b] Xin Li,[b] Himadri S. Samanta[b] and D. Thirumalai*[b]

Collective cell movement, characterized by multiple cells that are in contact for substantial periods of time and undergo correlated motion, plays a central role in cancer and embryogenesis. Recent imaging experiments have provided time-dependent traces of individual cells, thus providing an unprecedented picture of tumor spheroid growth. By using simulations of a minimal cell model, we analyze the experimental data that map the movement of cells in a fibrosarcoma tumor spheroid embedded in a collagen matrix. Both simulations and experiments show that cells in the core of the spheroid exhibit subdiffusive glassy dynamics (mean square displacement, $\Delta(t) \approx t^{\alpha}$ with $\alpha < 1$), whereas cells in the periphery exhibit superdiffusive motion, $\Delta(t) \approx t^{\alpha}$ with $\alpha > 1$. The motion of most of the cells near the periphery is highly persistent and correlated directional motion due to cell doubling and apoptosis rates, thus explaining the observed superdiffusive behavior. The α values for cells in the core and periphery, extracted from simulations and experiments, are in near quantitative agreement with each other, which is surprising given that no parameter in the model was used to fit the measurements. The qualitatively different dynamics of cells in the core and periphery is captured by the fourth order susceptibility, introduced to characterize metastable states in glass forming systems. Analyses of the velocity autocorrelation of individual cells show remarkable spatial heterogeneity with no two cells exhibiting similar behavior. The prediction that α should depend on the location of the cells in the tumor is amenable to experimental testing. The highly heterogeneous dynamics of cells in the tumor spheroid provides a plausible mechanism for the origin of intratumor heterogeneity.

1 Introduction

Collective cell movement, involving a group of cells that are spatially adjacent and display coherent motion for long periods, controls many processes such as embryogenesis, tumorigenesis, and wound healing.[1,2] A number of factors, including intercellular interactions, cell division and apoptosis, regulate the collective movement of cells.[1–8] In particular, the breakdown of strict cellular homeostasis between cell division and apoptosis, which regulates tissue development and maintenance, could be a root cause of a number of cancers.[9,10] Cancer metastasis is driven by migration of cells from the location of the primary tumor to secondary sites.[5] There could be multiple mechanisms underlying the migratory or invasive potential of cells.[1] However, elucidation of these mechanisms is difficult because of the highly coordinated and many body

nature of their movement.[2,11] To decipher the migration of tumor cells into the surrounding matrix, experimentalists have studied individual cell dynamics in an evolving three-dimensional (3D) growing spheroid *in vitro*[12–15] using a variety of imaging techniques. Typically, the spheroid is embedded in a collagen or extracellular matrix to mimic *in vivo* conditions.[15–19] These experiments have given direct glimpses of cell dynamics, which could be exploited to develop and test theoretical concepts in describing collective motion.

A number of theoretical studies have reported different scenarios for the dynamics of cell motion. A pioneering study,[20] treating tissues using continuum elasticity theory supplemented by simulations showed that if the rates of cell division and apoptosis are equal in the steady state, then the long time dynamics is diffusive. In other words, the cell mean square displacement (MSD), which is measurable using imaging data, grows linearly with time. More recently, this prediction was confirmed using detailed computer simulations performed in two dimensions, which established fluid-like behavior if the birth and apoptosis rates are balanced in the steady state.[21]

[a] *Department of Physics, University of Texas at Austin, Austin, TX 78712, USA*
[b] *Department of Chemistry, University of Texas at Austin, Austin, TX 78712, USA.*
E-mail: dave.thirumalai@gmail.com

Thus, under these conditions, the cells undergo fluid-like diffusion in the long time limit in contrast to the dynamics in confluent tissues in which cell division and apoptosis are prohibited.[22]

A completely different scenario arises, due to non-equilibrium effects, if there is an imbalance between cell birth (k_b) and apoptosis (k_a) rates. Recently, we used simulations and theory to investigate the dynamics of cells in a growing three dimensional (3D) tumor in which k_b and k_a are unequal.[23,24] To model cancer tumor growth, we used $\frac{k_b}{k_a} \approx 20$. In addition to k_a and k_b and an appropriate short range cell–cell interaction, the cell dynamics depends on the microenvironment. In our model, the sensitivity to the microenvironment is expressed in terms of a dormancy criterion, determined by the local pressure (p_i) on the ith cell. If p_i exceeds a critical pre-assigned value p_c, the cell becomes dormant until a time when $p_i < p_c$. The dormancy criterion serves as a mechanical feedback that limits the growth of the tissue.[25–28] We predicted that for this model, the dynamics of the cells is spatially heterogeneous. The cells exhibit highly persistent super-diffusive dynamics near the tumor periphery and subdiffusive glass-like dynamics in the core.

Here, we analyze imaging data of a growing 3D spheroid[15] using our theoretical framework. We show that predictions of our model quantitatively capture the salient features noted in the experiment. There is a marked difference in the dynamics of cells in the core of the solid tumor compared to those at the periphery. Typically, the cells in the core exhibit a glass-like dynamics characterized by subdiffusive motion (MSD increases sub linearly with time) while those at the periphery undergo superdiffusive motion (MSD increases as a power law with an exponent that is greater than unity). More importantly, the simulation results allow us to show that the dynamics of individual fibrosarcoma cells imaged in experiments also exhibit spatially heterogeneous dynamics across the entire tumor. The extent of heterogeneity varies both spatially and temporally. This is also reflected in the length scale dependent fourth order susceptibility, introduced in the context of spin glasses and structural glasses,[29] showing a peak for cells in the periphery whereas such a peak is absent for cells in the core of the tumor or it appears at extremely long times. The velocity correlations for the cells in the core persist over multiple cell divisions. Remarkably, the massive heterogeneity is manifested in the velocity correlation of individual cells, which renders averages meaningless. This key finding has implications for observation of intratumor heterogeneity.[30–32] Comparison between experimental data and simulations, which were performed without adjusting the model to fit the data, clearly shows that collective cell motion exhibits a high degree of spatial heterogeneity. We argue that massive spatial and temporal heterogeneity could be a universal characteristic in collective cell dynamics, determined only by an imbalance in birth and apoptotic rates and mechanical feedback-driven tumor evolution provided the interactions between cells are short-ranged.

2 Methods

Experimental data

We analyzed the imaging data of the fibrosarcoma cells[15] growing in a collagen matrix using simulations of a minimal model for tumor growth.[33,34] It is important to describe briefly the relevant experimental details in order to appreciate that the model used in our simulations (explained in the next section) is adequate to provide insights into the experimental data. In the experiments, a HT 1080 (human fibrosarcoma cell line) spheroid, with an initial radius of 174 μm, was embedded in a three-dimensional collagen matrix to mimic *in vivo* conditions. The spheroids were grown over 7 days and the trajectories of a few cells (10% cells were labelled with enhanced green fluorescent protein) were tracked. The equatorial plane of the spheroid was imaged at low magnification (10×) with a Nikon swept field microscope, and the cells were tracked every 14 minutes for 8 hours (using Metamorph image recognition software) on day 3, 5 and 7 of spheroid growth. The number of cells tracked on day 3, 5 and 7 was 145, 157 and 150 respectively. The data comprise the 2D projection of the 3D cell trajectory with the assumption that motion is isotropic in all directions. We were given only the x,y coordinates of individual cell trajectories. For this work, we analyzed the data mainly for day 7 unless mentioned explicitly. The fibrosarcoma cells divide every $\tau_{fib} = 21$ hours, which implies that the tumor spheroid grew over 8 cell cycles. At the end of day 7, the radius of the tumor, R_o, was approximately 3 mm.

Simulations

We briefly describe the simulation methods, which we developed previously.[23,35] We simulated a 3D growing tumor using an off-lattice model adopted from previous studies[33,34] where cells are considered as interacting soft deformable spherical particles that grow stochastically in time and divide into daughter cells on reaching a critical radius. The two body interactions between the cells are short ranged, consisting of two terms, a repulsion one (elastic force) and an attraction one (adhesion). The magnitude of the elastic force (F_{ij}^{el}) between two cells of radii R_i and R_j is given by

$$F_{ij}^{el} = \frac{h_{ij}^{3/2}}{\frac{3}{4}\left(\frac{1-\nu_i^2}{E_i} + \frac{1-\nu_j^2}{E_j}\right)\sqrt{\frac{1}{R_i(t)} + \frac{1}{R_i(t)}}}, \qquad (1)$$

where E_i and ν_i are the elastic modulus and Poisson ratio of the ith cell. The overlap distance between the two cells is denoted by h_{ij}. The adhesive interaction (F_{ij}^{ad}) is given by

$$F_{ij}^{ad} = A_{ij} f^{ad} \frac{1}{2}\left(c_i^{rec} c_j^{lig} + c_i^{lig} c_j^{rec}\right), \qquad (2)$$

where A_{ij} is the overlap area between the two interacting cells and f^{ad} determines the strength of the adhesive bond ($c_i^{rec} = c_i^{lig} = 1$). The net force ($\mathbf{F}_i$) on the ith cell is the vectorial sum of elastic and adhesive forces that the neighboring cells exert on it. We performed overdamped dynamics simulations without thermal noise because the matrix viscosity is assumed to be large.

Therefore, the equation of motion is taken to be $\dot{\mathbf{r}}_i = \dfrac{\mathbf{F}_i}{\gamma}$, where γ is the friction term that models the matrix as a thick gel and $\mathbf{r}_i$ is the position of the ith cell.

In the simulations, the cells grow stochastically and divide on reaching a critical radius. The growth of the ith cell is dependent on the microenvironment, which is determined by the pressure p_i exerted by neighboring cells. If p_i is smaller than a pre-assigned critical value, p_c, the cell grows in size. However, if $p_i > p_c$, the ith cell becomes dormant. The cell can switch between the dormant and growth mode depending on the ratio of $\dfrac{p_i}{p_c}$. The cell volume grows stochastically in time and it divides into two daughter cells (volume is conserved during cell division) on reaching a critical size. The growth of a cell is controlled by cell cycle time ($\tau_{\min}$), which was taken to be 15 hours. Apoptosis can also take place in the simulations where a cell is randomly removed. The apoptosis rate is given by $k_a = 10^{-6}$ s^{-1}. Because $k_a \ll \dfrac{1}{\tau_{\min}}$, we are simulating a growing system. Note that the cell cycle times in experiments (τ_{fib} = 21 hours) and simulations ($\tau_{\min}$ = 15 hours) are comparable. It should be stressed that neither $\tau_{\min}$ nor any other parameter was tweaked to obtain agreement with the experimental data.

We initiated the simulations by placing 100 cells whose x, y, z coordinates were chosen from a normal distribution with zero mean and a standard deviation of 20 μm. The simulated tumor spheroid was evolved for 600 000 s or 11.1 $\tau_{\min}$. The trajectories of all the cells were recorded and analyzed in order to calculate dynamical observables that shed light on the heterogeneity.

Classification of core and periphery

We arbitrarily classified cells as belonging to the core (periphery) if their distance from the center, R_c, is less (greater) than 1.5 mm (2 mm). Similarly, in simulations, cells with $R_c < 30$ μm are classified as belonging to the core whereas cells with $R_c > 60$ μm, are assumed to be in the periphery. The only purpose of performing this analysis is to show that, on average, the cell dynamics changes from the core to periphery.

3 Results

Sub-diffusive core and super-diffusive periphery

We first discuss our analysis of the experimental data. Given the small number of cells (150) imaged in the experiment,[15] we divided the cells into two parts based on their distances from the center of the spheroid (R_c) (see the left inset in Fig. 1a). We classified cells as belonging to the core (periphery) if their distance from the center, R_c, is less (greater) than 1.5 mm (2 mm). Since, imaging the cells in the core of a spheroid is technically difficult, there are fewer cells (27) in the core compared to those in the periphery (100). Mean Squared Displacement (MSD), $\Delta(t)$, is one of the metrics that can be readily

evaluated from single particle trajectories.[36] We evaluated $\Delta(t - t_i, t_i)$ using

$$\Delta(t - t_i, t_i) = \frac{1}{N_c} \sum_{k=1}^{N_c} [\mathbf{r}_k(t) - \mathbf{r}_k(t_i)]^2, \qquad (3)$$

where N_c is the number of cells that belong to either the periphery or the core, and $\mathbf{r}_k(t)$ is the position of cell k at time t. We denote t_i as the time when measurement of the cell trajectory begins, and t represents the time of spheroid growth. In calculating $\Delta(t)$, we did not perform any time average because the spheroid is far from equilibrium, which could imply that the behavior of $\Delta(t)$ might depend on the type of averaging performed.[37]

In general, we expect that $\Delta(t) \approx t^{\alpha}$. If $\alpha < 1$, then the dynamics is subdiffusive, which could be suggestive of glass-like behavior. For a fluid-like motion, $\alpha = 1$. If α exceeds unity, then the dynamics would be superdiffusive. Fig. 1a shows that cells in the tumor core undergo subdiffusive dynamics with $\alpha = 0.66$. In contrast, fibrosarcoma cells in the peripheral region undergo superdiffusive dynamics with $\alpha = 1.34$ (see the right inset of Fig. 1a for fits to log($\Delta(t)$) $vs.$ log(t), the slope of which determines α).

In order to understand the spatially heterogeneous anomalous diffusion in a growing spheroid (Fig. 1a), we simulated a freely expanding cell colony in 3D using the methods described elsewhere.[23,33,34] We divided the simulated tumor spheroid into the core and periphery. In the simulated tumor, cells with $R_c < 30$ μm are classified as belonging to the core whereas cells with $R_c > 60$ μm are assumed to be in the periphery. There exists a substantial length scale difference in what we define as periphery and core in simulations as compared to experiments because the size of the spheroid is on the order of mm in experiments whereas the simulated spheroid reaches sizes on the order of ≈ 0.2 mm. However, the simulations capture the experimental findings well. For the two spatial regions, we calculated $\Delta(t)$ for cells as was done for the experiments (Fig. 1a). Fig. 1b shows that in the limit $t > \tau_{\min}$, the MSD for cells in the interior is subdiffusive with $\alpha = 0.58$, whereas the cells at the periphery exhibit superdiffusive behavior with $\alpha = 1.52$. The plot was generated by tracking cells that were present in the simulation (note that cells can undergo apoptosis in simulations) between initial time $t_i \approx \tau_{\min}$ and the final time $t_f \approx 11.1\tau_{\min}$ where $\tau_{\min} = 54\,000$ s. We averaged the calculations over 50 such simulations. The α values extracted from simulations are in near quantitative agreement with experiments, which is remarkable given that no parameter in the model was adjusted to describe the experiments. Both experiments and simulations show that the cells at the tumor core display glass-like behavior ($\alpha < 1$) and those in the periphery exhibit superdiffusive ($\alpha > 1$) behavior.

Spatial variations in the cell motilities

The quantitative agreement of α values with experiments allows us to use simulations to provide nuanced analyses of the cell trajectories. We sub-divided the simulated tumor spheroid into
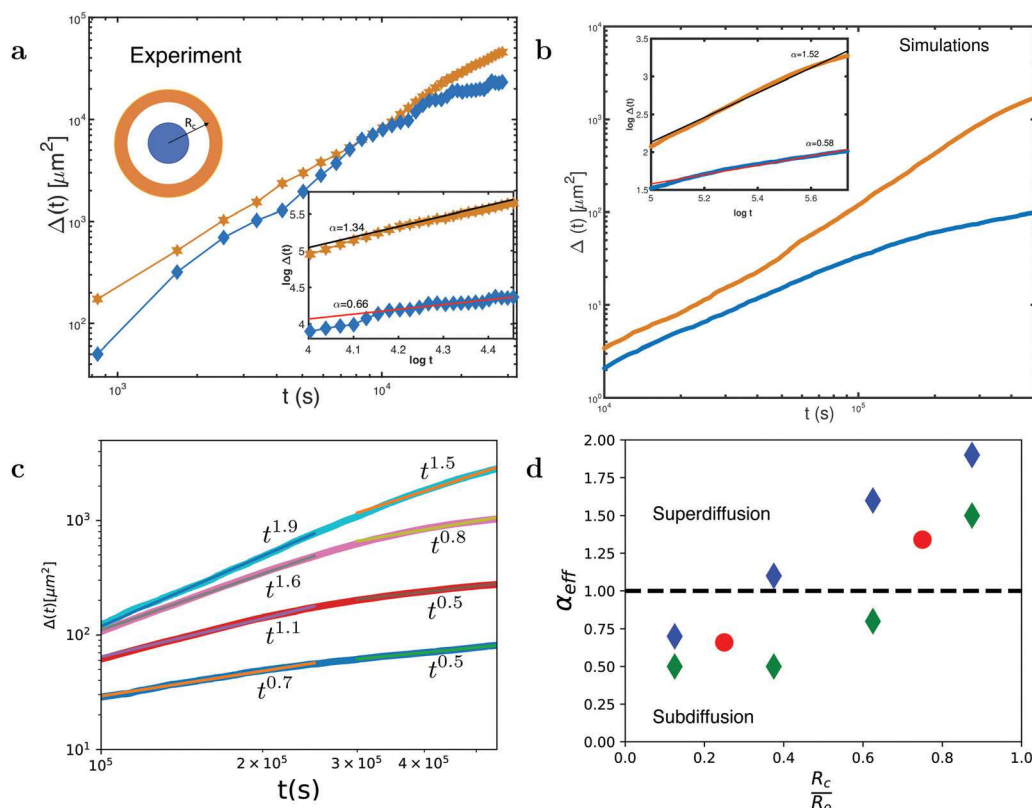
Fig. 1 Spatial variation in dynamics. (a) Mean squared displacement ($\Delta(t)$) as a function of time for experimentally tracked cells in the core (blue) and periphery (orange) of a growing spheroid. The measurements[15] were performed on day 7 of the growth. A schematic of the core and periphery in terms of R_c is shown in the upper left. The blue line shows the MSD for cells in the core ($R_c < 1.5$ mm) and the orange line depicts the MSD for cells in the periphery ($R_c > 2$ mm). The inset shows the plot for $\log(\Delta(t))$ *vs.* $\log(t)$ for cells in the core and periphery, where the periphery MSD has been multiplied by a factor of 10 for clarity. The slope of the curve $\log(\Delta(t))$ *vs.* $\log(t)$, is the value of α in the equation $\Delta(t) \approx t^\alpha$. The black (red) line in the inset shows the power law fit yielding $\alpha = 1.34$ (0.66). (b) Same as (a) except $\Delta(t)$ has been calculated using simulations. The orange line shows the MSD of the periphery cells ($R_c > 60$ μm) whereas the blue line corresponds to the MSD of the cells in the core ($R_c < 30$ μm). The values of α are in black (red) for cells in the periphery (core). (c) MSD of cells in different layers in the growing spheroid calculated using simulations. From bottom to top, the MSD curves are for cells whose distance from the center of the spheroid (R_c) is 0 μm $< R_c < 25$ μm, 25 μm $< R_c < 50$ μm, 50 μm $< R_c < 75$ μm and 75 μm $< R_c < 100$ μm. The curves were fitted by dividing time into two intervals: the first corresponds to 10^5 s $< t < 2.5 \times 10^5$ s, and the second covers 3×10^5 s $< t < 5.5 \times 10^5$ s. The effective exponent values (α_{eff}) were calculated using $\Delta(t) \approx t^{\alpha_{eff}}$. The values of α_{eff} are given next to the curves. (d) Plot showing $\alpha_{eff}^{T_{w1}}$ for T_{w1} and $\alpha_{eff}^{T_{w2}}$ for T_{w2} as a function of $\frac{R_c}{R_o}$ (R_o is the radius of the tumor defined in the text) for experiments (red disks) and simulations (blue diamond for the shorter time interval, and green diamond for the longer time interval). The dashed black line is the line where $\alpha = 1$ below (above), which denotes sub-diffusive (super-diffusive) motion.

four layers arbitrarily, and calculated $\Delta(t)$ for cells in each layer. The thickness of each layer is roughly 25 μm. We performed statistical averages using cells that were in the simulations between time τ_{min} and $11\tau_{min}$. In Fig. 1c, the time dependencies of $\Delta(t)$ are plotted for 4 layers. The results in Fig. 1c reveal two interesting aspects of the nature of cell motility inside a growing spheroid. (a) The $\Delta(t)$ curves exhibit a non-uniform curvature on the timescale ($\approx 10\tau_{min}$). Nevertheless, to illustrate the spatial variations in the cell motilities, we fit the $\Delta(t)$ curves by a power law by dividing the total time into two intervals. One spans $T_{w1} = 10^5$ s $< t < 2.5 \times 10^5$ s and the other covers $T_{w2} = 3 \times 10^5$ s $< t < 5.5 \times 10^5$ s. The fits in both the time intervals reveal an enhancement in the cell motility as one moves from core to periphery. The extracted effective exponents $\left(\alpha_{eff}^{T_{w1}} \text{ and } \alpha_{eff}^{T_{w2}}\right)$ show that the cell motility changes from sub-diffusive to super-diffusive as the distance from the center of the tumor increases. (b) The exponent values (Fig. 1c caption) in a given layer decrease $\left(\alpha_{eff}^{T_{w2}} < \alpha_{eff}^{T_{w1}}\right)$ as time advances because a cell in the periphery at a given time becomes part of the core at a later time. Thus, the values of α_{eff} are themselves time dependent, and their utility is to merely illustrate qualitatively the nature of the dynamics of the cells in an evolving tumor.

The calculated exponents $\alpha_{eff}^{T_{w1}}$ and $\alpha_{eff}^{T_{w2}}$ (obtained by fitting $\Delta(t) \sim t^{\alpha_{eff}}$ in the first and second time window of Fig. 1c) are shown in Fig. 1d. We scaled the x-axis by R_o, which is the approximate radius of the tumor spheroid. In experiments, $R_o \approx 3$ mm and for simulations, $R_o \approx 0.1$ mm. The prediction that the effective diffusion exponent varies spatially as the distance from the spheroid center increases can be tested in experiments if the number of imaged cells is increased. We believe that light sheet microscopy methods could be used to test our

predictions that the dynamics would change continuously from being jammed to exhibiting super-diffusive behavior.[17,38]

The van Hove function is non-Gaussian

The anomalous nature of the diffusion of cells inside the tumor spheroid can be gleaned by calculating the van Hove function ($P(\Delta x, \delta t)$), which gives the distribution of Δx obtained from

$$\Delta x_i = x_i(t + \delta t) - x_i(t), \qquad (4)$$

where $x_i(t)$ is the x coordinate of the ith cell at time t. Fig. 2 shows $P(\Delta x, \delta t)$, in which Δx has been time and ensemble averaged, for the cells tracked in experiments ($\delta t = 28$ min)
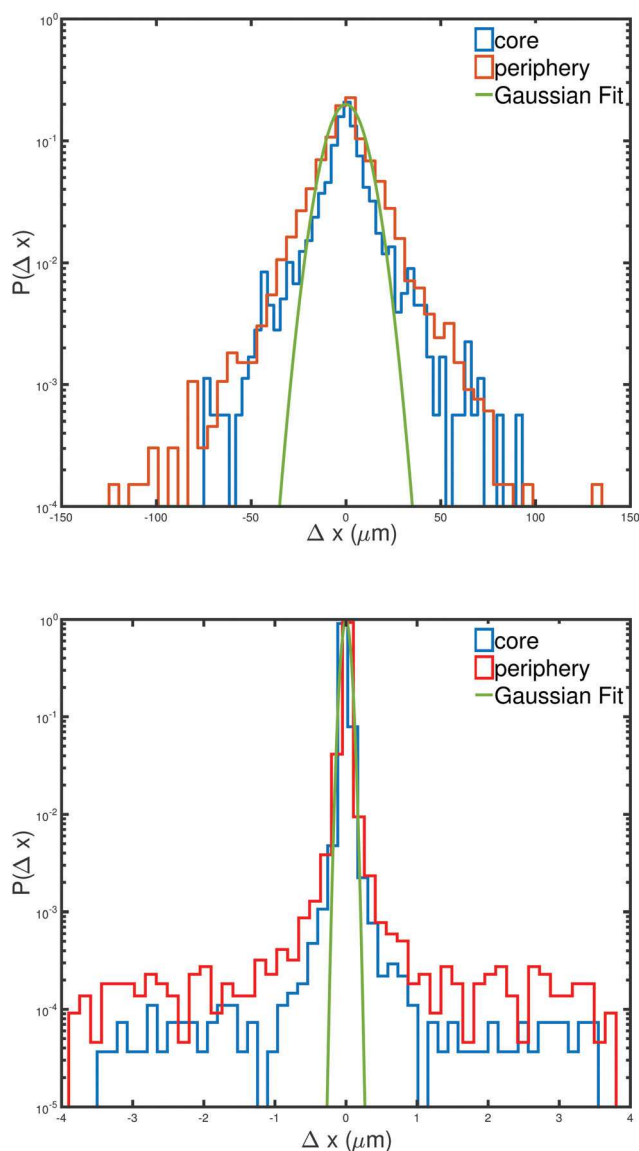

Fig. 2 Non-Gaussian behavior of cell displacements. (Top) van Hove function, ($P(\Delta x)$), for cells tracked in the experiments. The red (blue) line shows $P(\Delta x)$ for cells in the experiments. The green line is the Gaussian fit. (Bottom) $P(\Delta x)$ for cells tracked in simulations where the red (blue) line represents cells in the periphery (core). The green line is the Gaussian fit. There is a striking similarity, except for the length scale, between the simulation and experimental results.

and simulations ($\delta t = 10$ min). If the cells exhibited liquid-like dynamics, then $P(\Delta x, \delta t)$ would be a Gaussian function.[39] This expectation is in sharp contrast with the nature of cell movement seen in Fig. 2. For cells in both the regions, $P(\Delta x, \delta t)$ exhibits a fat tail in the distributions deviating substantially from Gaussian behavior. However, cells near the periphery take longer jumps, indicating the fast movement of these cells compared to cells in the core. As discussed elsewhere, this is a manifestation of dynamic heterogeneity.[40–42]

Superdiffusive exponent is invariant under time translation

A growing spheroid is a non-equilibrium system, which means that the values of any physical observable could depend in principle on the time of measurement. To test whether the MSD exponent α depends on the observation time when cell trajectories are measured, we calculated the time averaged MSD, $\Delta(t_d)$, on day 3, day 5 and day 7 of spheroid growth. Time averaged MSD is defined as

$$\Delta(t_d) = \frac{1}{N} \sum_{i=1}^{N} \left\langle [\mathbf{r}_i(t_d + t) - \mathbf{r}_i(t)]^2 \right\rangle_t, \qquad (5)$$

where N denotes the total number of cells tracked and $\langle \ldots \rangle_t$ refers to the time average. Fig. 3b shows $\Delta(t_d)$ measurements on days 3, 5 and 7. To our surprise, the exponents are independent of time with $\alpha \approx 1.4$. This might mean that the tumor cells have not aged on the experimental time scale.

To ascertain if our simulations are in accord with the analysis of the experimental data, we calculated the time averaged MSD during different time periods of spheroid growth. Fig. 3a shows the snapshots of simulations at $t = 3\tau_{min}$, $t = 5\tau_{min}$, $t = 7\tau_{min}$ and $t = 11\tau_{min}$. In the simulations, we considered cell trajectories for three time periods as done in experiments. The three periods were $3\tau_{min} < t < 4\tau_{min}$, $5\tau_{min} < t < 6\tau_{min}$ and $7\tau_{min} < t < 8\tau_{min}$. The averaging was performed over all the cells that were present both at the beginning and at the end of measurement. Fig. 3c shows the behavior of time averaged MSD during the three time intervals. Our simulations show the same behavior as obtained in experiments, with $\alpha = 1.37$ for measurements during the three time intervals.

Self-overlap function and fourth order susceptibility

The extent of spatially heterogeneous dynamics can be further quantified using the self overlap function ($\Omega(l, t_d)$)[43,44]

$$\Omega(l, t_d) = \frac{1}{N_c} \sum_{i=1}^{N_c} \Omega_i(l, t_d), \qquad (6)$$

where N_c is the number of cells in the core or periphery of the tumor spheroid, t_d is the delay time, and l is the characteristic length scale associated with the overlap function $\Omega(l, t_d)$. The overlap function for the ith cell is given by

$$\Omega_i(l, t_d) = \langle \Omega_i(l, t_d, t) \rangle_t, \qquad (7)$$

where $\langle \cdots \rangle_t$ is an average over time. We calculated $\Omega_i(l, t_d, t)$ using

$$\Omega_i(l, t_d, t) = \Theta(l - |\mathbf{r}_i(t + t_d) - \mathbf{r}_i(t)|). \qquad (8)$$
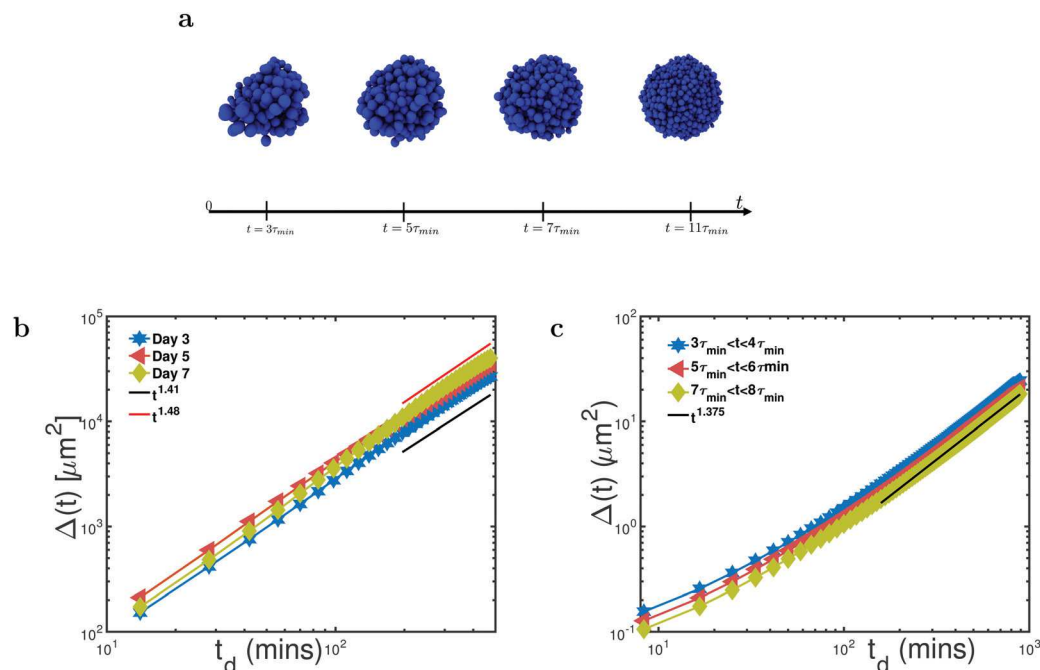
Fig. 3 The long time MSD exponent is approximately independent of time in a growing spheroid. (a) Snapshots from the simulations showing the growth of the tumor spheroid. The leftmost snapshot is taken at $t = 3\tau_{min}$ (≈ 500 cells), followed by $t = 5\tau_{min}$ (≈ 1200 cells), $t = 7\tau_{min}$ (≈ 2200 cells) and $t = 11\tau_{min}$ (≈ 6000 cells). The black line below denotes the time axis with labels denoting the time of the snapshot. (b) Time averaged $\Delta(t)$ for experimentally tracked cells on days 3, 5 and 7. The blue line corresponds to day 3, the red line corresponds to day 5 and the green line corresponds to day 7. The black and red lines show power law exponents of 1.41 and 1.48, respectively. (c) Time averaged $\Delta(t)$ of simulated cells for 3 observation times. The blue line corresponds to the observation time of $3\tau_{min} < t < 4\tau_{min}$, red corresponds to the observation time of $5\tau_{min} < t < 6\tau_{min}$ and green corresponds to the observation time of $7\tau_{min} < t < 8\tau_{min}$. The black line corresponds to the power law exponent of 1.375.

The length, l, serves as the cutoff distance for which the Heaviside function ($\Theta(l - |\mathbf{r}_i(t + t_d) - \mathbf{r}_i(t)|)$) is equal to unity (zero), if l is greater (smaller) than $|\mathbf{r}_i(t + t_d) - \mathbf{r}_i(t)|$. Thus, $\Omega_i(l,t_d)$ measures the degree of movement of cells in the time t_d. We first calculated $\Omega(l,t_d)$ using the experimental imaging data. Fig. 4a shows the difference in the decay of $\Omega(l,t_d)$ of the cells in the core ($R_c < 1.5$ mm) and the periphery ($R_c > 2$ mm). The value of l was chosen as 100 μm because on this length scale, the difference between the dynamics of the interior and periphery cells are vivid (see Fig. 1a). Fig. 4a shows the stark difference in the dynamics of cells in the core, which exhibit a slow dynamics compared to cells near the tumor boundary, which is also reflected in Fig. 1a. The plot of $\Omega(l,t_d)$ for cells in the periphery was fitted to an exponential function $\left(A e^{-\frac{t_d}{\tau}} \right)$, which yielded $\tau = 0.3\tau_{fib}$ (τ_{fib} is the cell doubling time of the fibrosarcoma cells).

We also calculated $\Omega(l,t_d)$ from simulations using $l = \frac{10}{3}$ μm, which is small compared to $l = 100$ μm, due to the difference in spheroid sizes. However, the length scale, l, in both experiments and simulations satisfies the criterion $\left(\frac{l}{R_o} \right)_E = \left(\frac{l}{R_o} \right)_S$, where R_o is the radius of the tumor, and the subscripts E and S refer to experiments and simulations, respectively. With this criterion, the experimental and simulation results could be compared on an equal footing. As mentioned earlier, R_o for experiments is 3 mm and for simulation, it is 0.1 mm.

Fig. 4b shows the difference in the overlap function of cells in the interior ($R_c < 30$ μm) and the periphery region ($R_c > 60$ μm) for the simulated tumor spheroid. The behavior of the overlap function calculated in simulations qualitatively matches with the experiments for the core cells. The exponential fit for the decay of $\Omega(l,t_d)$ $\left(A e^{-\frac{t_d}{\tau}} \right)$ yielded $\tau_p = 0.6\tau_{min}$ and $\tau_c = 3.2\tau_{min}$ for the cells in the core and periphery, respectively. The decay time, τ, for the cells in the periphery, obtained using simulations ($\tau_p = 0.6\tau_{min}$) is in good agreement with the experiments ($\tau = 0.3\tau_{fib}$). However, it is difficult to compare the behavior of $\Omega(l,t_d)$ for cells in the core between experiments and simulations because the cells were not imaged for a sufficient time in the experiments (the $\Omega(l,t_d)$ curve does not decay substantially). For cells in the core, the relaxation time $\tau_c = 3.2\tau_{min}$ (see Fig. 4b obtained from simulations) is six times longer than τ_p $\left(\frac{\tau_c}{\tau_p} \approx 6 \right)$. Hence, we hypothesize that the imaging needs to be performed for at least six times longer than the current observation time to observe the relaxation of $\Omega(l,t_d)$ for cells in the core.

Spatial variations in $\Omega(l,t_d)$

We sub-divided the tumor spheroid into multiple layers and calculated $\Omega(l,t_d)$ for cells in a given layer. Fig. 4c shows the dependence of $\Omega(l,t_d)$ as a function of distance from the center of the spheroid. The cells in the inner most layer exhibit very
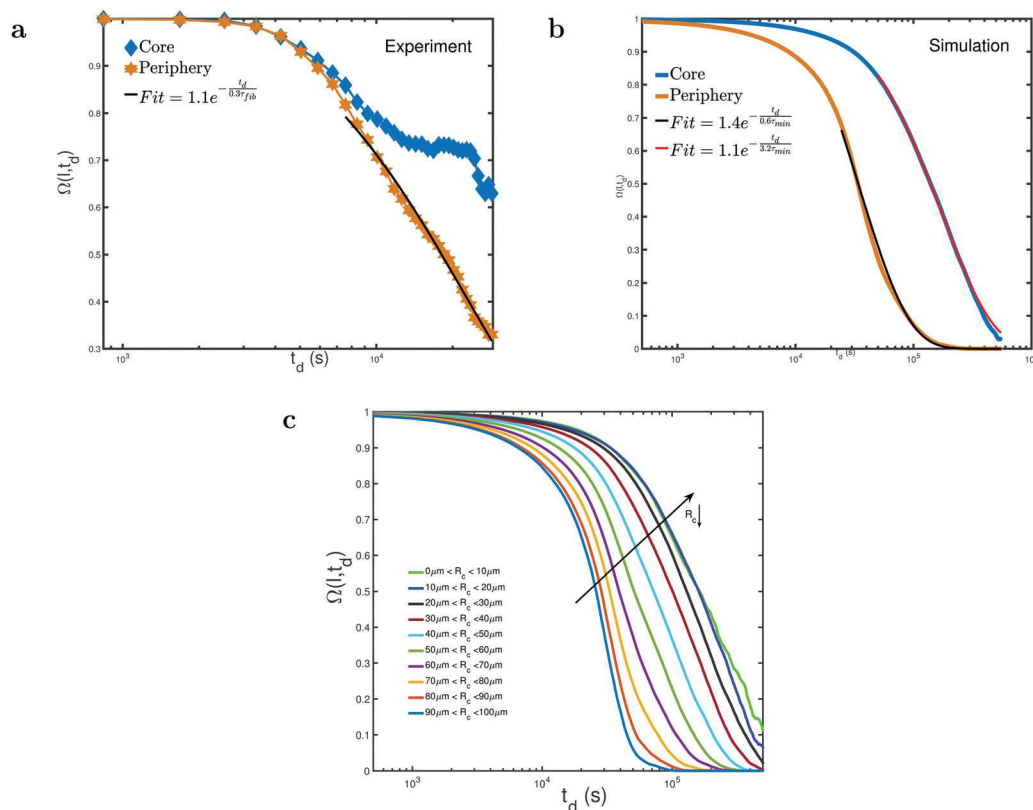
Fig. 4 (a) Self-overlap function ($\Omega(l,t_d)$) for experimentally tracked cells as a function of delay time t_d with l = 100 μm. The orange line shows the overlap function for cells near the periphery (R_c > 2 mm) and the blue line represents cells in the core (R_c < 1.5 mm). The black line is an exponential fit. (b) Self-overlap function for simulated cells as a function of delay time t_d with $l = \frac{10}{3}$ μm. The orange line shows $\Omega(l,t_d)$ for periphery cells (R_c > 60 μm) whereas the blue line corresponds to $\Omega(l,t_d)$ for cells in the core (R_c < 30 μm). (c) Time dependence of $\Omega(l,t_d)$ for cells in different layers of the spheroid. From top to bottom, $\Omega(l,t_d)$ curves are for cells whose distance from the center of spheroid (R_c) is $10(i − 1)$ μm < R_c < $10i$ μm, for all i = {1,2,...,10}. The dashed arrow indicates the decreasing distance from the center of the tumor spheroid along its direction (R_c↓).

slow glass-like dynamics compared to those in the outermost layer. In order to further distinguish between the slow and fast dynamics in different layers in the spheroid, we calculated the fourth order susceptibility ($\chi_4(l,t_d)$),[29]

$$\chi_4(l,t_d) = N_c[\langle \Omega_i(l,t_d,t)^2 \rangle - \langle \Omega_i(l,t_d,t) \rangle^2]. \qquad (9)$$

Fig. 5a and b show $\chi_4(l,t_d)$ as a function of t_d for cells in the core and periphery in experiments and simulations, respectively. Both figures show qualitatively identical behavior with cells in the periphery exhibiting a peak in $\chi_4(l,t_d)$. We should note that in simulations, $\chi_4(l,t_d)$ for cells in the core exhibits a peak, which is absent in the experiments. As explained earlier, this is because the peak in $\chi_4(l,t_d)$, which usually appears when $\Omega(l, t_{peak}) = \frac{1}{e}$, for cells in the core would occur at longer time scales $\left(\frac{\tau_c}{\tau_p} \approx 6 \right)$.

To understand the behavior of $\chi_4(l,t_d)$ as a function of R_c, we sub-divided the simulated tumor spheroid into several layers. Fig. 5c shows the behavior of $\chi_4(l,t_d)$ for cells as a function of distance from the center of the spheroid (R_c). We note two interesting aspects from the behavior of $\chi_4(l,t_d)$. Firstly, the position of the peak in $\chi_4(l,t_d)$, which corresponds to the

maximal heterogeneity in the movement of cells on the length scale l, shifts to the right due to the slow dynamics as we approach the center of the tumor spheroid. Secondly, the amplitude of the peak in $\chi_4(l,t_d)$, which corresponds to the growing dynamical correlation length,[45] initially increases (see inset of Fig. 5c) and then decreases as a function of distance from the spheroid.

Cells in the periphery undergo directed and highly persistent motion

The massively heterogeneous nature of cell motility within a single tumor spheroid can be highlighted using the time-dependent changes in the trajectories of individual cells. We first analyzed the directionality of individual cell movement as a function of distance from the center of spheroid (R_c) by calculating the straightness index (SI),[46]

$$\text{SI}(R_c) = \frac{1}{N_r} \sum_{i=1}^{N_r} \frac{|\mathbf{r}_i(t_f) - \mathbf{r}_i(t_i)|}{\sum |\delta\mathbf{r}_i(t)|}. \qquad (10)$$

The numerator in the above equation is the magnitude of the net displacement of the ith cell between time t_i and time t_f. The denominator is the total length of the trajectory of the ith cell, and N_r is the number of cells between R_c and $R_c + \delta R_c$.
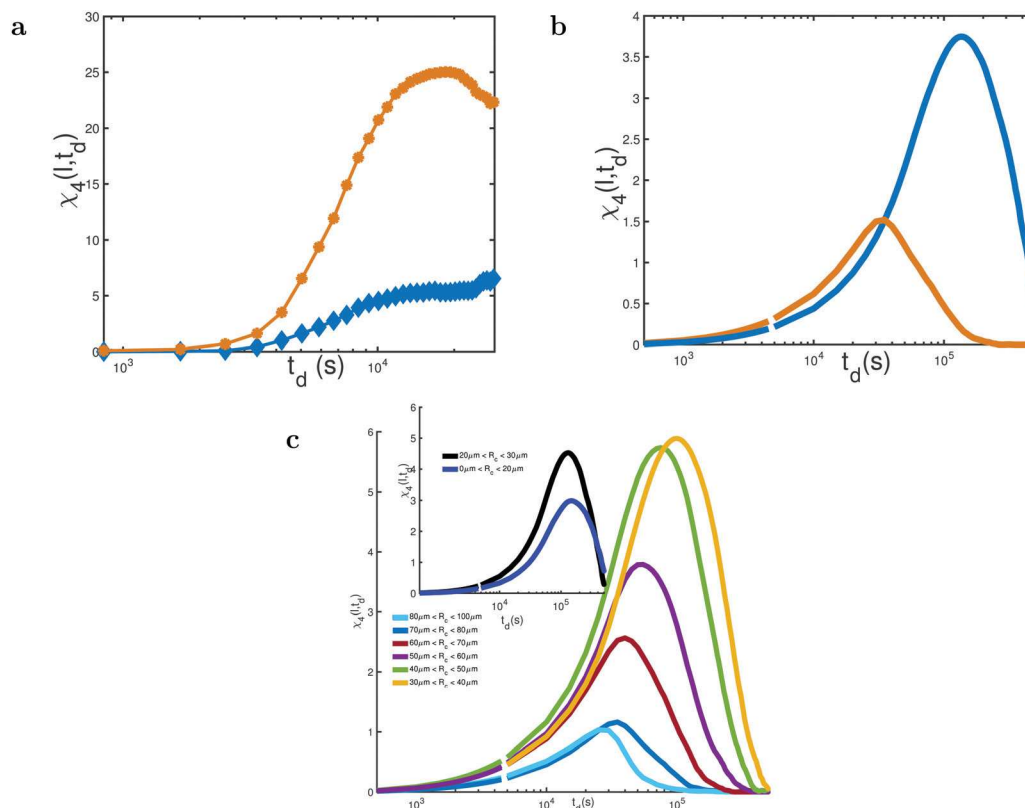
Fig. 5 (a) Fourth order susceptibility ($\chi_4(l,t_d)$) determined by the variance in $\Omega(l,t_d)$ for experimentally tracked cells. $\chi_4(l,t_d)$ for cells in the core (periphery) is shown in blue (orange). (b) $\chi_4(l,t_d)$ for cells tracked in simulations. Blue (orange) line shows $\chi_4(l,t_d)$ for cells in the core (periphery). (c) Layer by layer fourth order susceptibility ($\chi_4(l,t_d)$) determined by variance in $\Omega(l,t_d)$. From top to bottom (except the innermost layer shown in sky blue), $\chi_4(l,t_d)$ curves for cells whose distance from the center of spheroid (R_c) is $10(i-1)$ μm $< R_c < 10i$ μm, for all $i = \{4,...,8\}$. The innermost layer corresponds to 80 μm $< R_c < 100$ μm. In the inset, the black (blue) curve corresponds to $\chi_4(l,t_d)$ for 20 μm $< R_c < 30$ μm (0 μm $< R_c < 20$).

For experiments, $\frac{\delta R_c}{R_o} = 0.14$ whereas $\frac{\delta R_c}{R_o} = 0.1$ for simulations. If SI is unity, then the cells move along a perfectly straight trajectory. Fig. 6a, which displays the straightness of trajectories of cells calculated using experimental data in a growing spheroid on day 7 during 8 hours of imaging, shows clearly that straightness of the trajectory increases as the distance of the cell from the spheroid core increases. We also evaluated SI (R_c) (see Fig. 6b) in the simulations using $t_i = \tau_{min}$ and $t_f = 11.1\tau_{min}$. The behavior of SI (R_c) agrees well with the trends observed in the experiments. The cells in the core (periphery) have SI → 0 (SI → 1).

Massive spatially heterogeneous dynamics

To further illustrate the difference in the directed motility of cells in the periphery and the core, we calculated the persistence of individual cell movements in both experiments and simulations. We defined persistence ($P(t_d)$) using the velocity of the cells as

$$P(t_d) = \frac{1}{N_c}\sum_{i=1}^{N_c}\langle \hat{v}_i(t+t_d)\cdot\hat{v}_i(t)\rangle_t. \quad (11)$$

In eqn (11), $\hat{v}_i(t)$ is the unit velocity vector of the ith cell at time t, N_c is the number of cells in the spheroid core or the periphery, t_d is the delay time, and $\langle\cdots\rangle_t$ refers to the time average.

Fig. 6c and d show the $P(t_d)$ curves as a function of t_d calculated from experimental data and simulations, respectively. We calculated $P(t_d)$ from simulations using the cells that were present during the time interval of $10\tau_{min}$ and $11.1\tau_{min}$. Cells in the periphery move in a highly persistent (directed motion with hardly any decay in $P(t_d)$ as t_d changes) manner compared to cells in the interior. The results in these figures show dramatically that there are substantial cell-to-cell variations in $P(t_d)$ with no two cells exhibiting similar behavior. In particular, there is widespread heterogeneity in trajectories of individual cells (see $P(t_d)$ for individual cells, which are denoted by thin lines). This finding is also reminiscent of glassy systems, characterized by large subsample to subsample fluctuations within a single large sample of glass.[47] The results in Fig. 6c and d imply that averages, shown in dark colors, have no physical meaning, and could provide misleading information. The massively spatially heterogeneous dynamics of individual cells during collective movement might be a plausible mechanism for the origin of intratumor heterogeneity.[30–32]

4 Discussion

We have used simulations of a minimal model[23] to analyze experimental results[15] where individual cell trajectories were
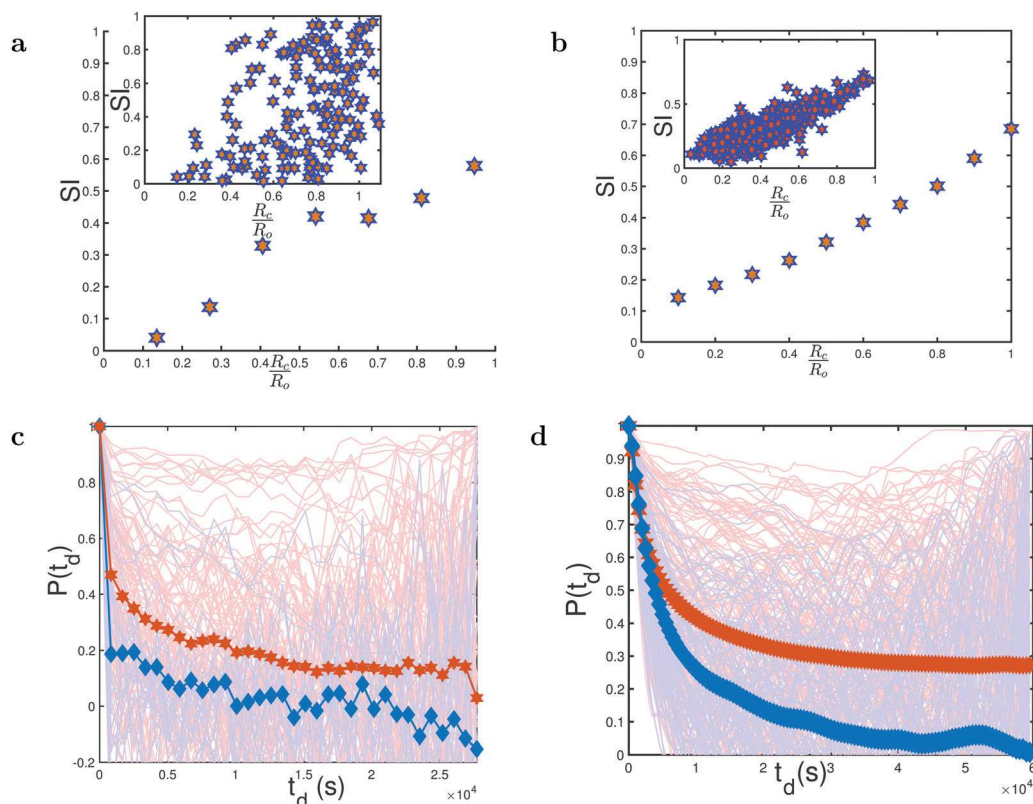
Fig. 6 (a) Straightness index (SI) of cells as a function of distance from the center of the spheroid $\left(\frac{R_c}{R_o}\right)$ obtained using the experimental data. The inset shows the scatter plot of SI *vs.* $\frac{R_c}{R_o}$ for all cells tracked. The plot in the main figure was generated by binning the data in the inset. (b) SI for the simulated cells as a function of distance. The inset shows the SI for all the cells. The data in the inset were binned to generate the main figure. (c) Persistence $(P(t_d))$ function defined as $\langle \hat{v}(t + t_d) \cdot \hat{v}(t) \rangle_t$ for experimentally tracked cells. The red line depicts $P(t_d)$ for cells in the periphery ($R_c > 2$ mm) and blue line shows the $P(t_d)$ for cells in the core ($R_c < 1.5$ mm). The red and blue thin lines are $P(t_d)$ for individual cells. (d) $P(t_d)$ for simulated cells. The red (blue) line depicts $P(t_d)$ for cells in the periphery (core). The red (blue) thin lines are $P(t_d)$ for individual cells in the periphery (core). (d) $P(t_d)$ for simulated cells with red line for cells in the periphery ($R_c > 60$ μm) whereas blue line is for cells in the core ($R_c < 30$ μm). The red and blue thin lines are $P(t_d)$ for individual cells. In both experiments and simulations, there are substantial heterogeneities among individual cells.

monitored using fluorescence microscopy in a tumor spheroid embedded in a 3D collagen matrix. Remarkably, without adjusting any parameter in the model to obtain agreement with the experiment, the exponents characterizing the mean square displacement of cells in the core and periphery are in quantitative agreement with values extracted from experimental data. This allowed us to dissect the remarkable spatial and temporal variations in the dynamics of the cells from the center to the periphery of the tumor. Both experiments and simulations unveil that in the peripheral region of the spheroid, cells exhibit highly persistent super-diffusive dynamics whereas the motion in the tumor interior is sub-diffusive.

The sluggish cell dynamics in the core is reminiscent of relaxation in supercooled liquids as they undergo a transition to a glassy state.[31] Using concepts from glass transition theory, we showed that higher order susceptibility of the cells near the tumor periphery in experiments, which are fully accounted for in the simulations, shows a peak at $t \approx 5.6$ hours – the approximate time at which coherent motion occurs. A similar calculation for the interior jammed cells shows a peak that is likely to be present at much longer time scales. The difference

in the fourth order susceptibility illustrates the spatial and temporal heterogeneity. Fuller analyses of the simulation results confirm that the dynamics is massively heterogeneous with substantial cell-to-cell variations. The dynamics of individual cells varies greatly depending on their spatial locations in the tumor. We predict that the exponents associated with the mean square displacement should change continuously as a function of cell distance from the center of the spheroid. This prediction, which already has partial support (see Fig. 1d), could be further tested by imaging experiments that track a much larger number than is currently possible.

The excellent agreement between simulations, which were not intended to model the specifics of the growth of fibrosarcoma tumor spheroid in a 3D collegen matrix, and experiments allows us to suggest generic mechanisms that govern the growth of spheroids. Besides the short-range cell–cell interactions, the parameters that control tumor expansion in our simulations are the asymmetry between cell birth (k_b) and apoptosis rates (k_a), and a dormancy factor that is expressed in terms of a pressure threshold that a cell experiences. The imbalance ($k_b \gg k_a$) produces self-generated active forces[48] that act in a directed

manner on cells that are close to the periphery, facilitating their persistent motion. Such forces in cells are related to myosin-based contractile stresses, which have been argued to be a major factor in directed growth.[15] Our previous study also suggested (see especially Fig. 14 in ref. 23) that there must be a high degree of correlation between the movement of neighboring cells at the tumor periphery. In other words, the super-diffusive behavior is a consequence of collective correlated motion of cells near the boundary. In an expanding tumor, there is an outward radial stress, arising from an imbalance between the rates of cell birth and apoptosis, which renders the cells on the periphery superdiffusive. Because these arguments are general, we propose that global dynamics of a growing spheroid must exhibit the features of super-diffusive motion in the periphery, jamming in the interior, and a high degree of spatial heterogeneity in the movement of individual cells. Finally, it is likely that the non-equilibrium dynamics, arising due to $k_b \gg k_a$, may also be relevant in other situations such as embryogenesis and wound healing.

A posteriori rationale for observing super-diffusive behavior is that there is a radial flow that thrusts the cells at the boundary outward. Although this is certainly correct, it should be noted that the force leading to the radial velocity is not explicitly described in the model but is self-generated by the birth and apoptotic processes.[23] Moreover, such a force, which is inherent to the physics of tumor growth in the model, has to be persistent in order to observe super-diffusive behavior (*i.e.*, act over several cell doubling times). Moreover, biologically relevant parameters $\left(p_c, \frac{k_b}{k_a}\right)$ could be chosen to entirely suppress the super-diffusive behavior even though the tumor expands. Thus, the dynamics in the model is a complex interplay between short range forces as well as the criterion for dormancy, and cell birth and apoptosis rates. It is worth emphasizing that the good agreement between our findings and the analysis of the experimental data implies that a similar mechanism is operative in the collective movement of fibrosarcoma cells against the collagen matrix. This, perhaps, is the major surprise in this study.

We have captured quantitatively the spatially heterogeneous dynamics of cells in a growing tumor. Analysis of the experimental data, which provide the time traces of a small number of individual cells,[15] reveals that the core cells exhibit sub-diffusive dynamics ($\Delta(t) \sim t^\alpha$, where $\alpha = 0.66$) and those near the periphery undergo super-diffusive dynamics ($\Delta(t) \sim t^\alpha$, where $\alpha = 1.34$). Remarkably, without adjusting any parameter, we predict that cells in the core (periphery) exhibit sub-diffusive (super-diffusive) dynamics with $\alpha = 0.57(1.52)$. Comparison with experiments shows that there is only one potential limitation. Due to differences in the size of the simulated and experimental tumor, we had to choose different length scales while comparing the overlap function and fourth order susceptibility. Nevertheless, the qualitative insights obtained from our work provide a way to explore the dynamics of tumor evolution by varying the parameters that are most relevant biologically (p_c, k_a and k_b). Using the velocity autocorrelation function, we revealed the massive dynamical heterogeneity of cells in an expanding tumor, which makes the notion of mean less relevant. This cell to cell variation is an example of phenotypic heterogeneity and our work will be important in providing a mechanism of the origin and maintenance of intratumor heterogeneity.

Conflicts of interest

There are no conflicts to declare.

References

1 P. Friedl and D. Gilmour, *Nat. Rev. Mol. Cell Biol.*, 2009, **10**, 445.
2 A. G. Clark and D. M. Vignjevic, *Curr. Opin. Cell Biol.*, 2015, **36**, 13–22.
3 D. Ingber, *Ann. Med.*, 2003, **35**, 564–577.
4 F. Guilak, D. M. Cohen, B. T. Estes, J. M. Gimble, W. Liedtke and C. S. Chen, *Cell Stem Cell*, 2009, **5**, 17–26.
5 S. Kumar and V. M. Weaver, *Cancer Metastasis Rev.*, 2009, **28**, 113–127.
6 W. G. Stetler-Stevenson, S. Aznavoorian and L. A. Liotta, *Annu. Rev. Cell Biol.*, 1993, **9**, 541–573.
7 D. T. Tambe, C. C. Hardin, T. E. Angelini, K. Rajendran, C. Y. Park, X. Serra-Picamal, E. H. Zhou, M. H. Zaman, J. P. Butler and D. A. Weitz, *et al.*, *Nat. Mater.*, 2011, **10**, 469.
8 M. C. Marchetti, J.-F. Joanny, S. Ramaswamy, T. B. Liverpool, J. Prost, M. Rao and R. A. Simha, *Rev. Mod. Phys.*, 2013, **85**, 1143.
9 B. Barres, I. Hart, H. Coles, J. Burne, J. Voyvodic, W. Richardson and M. Raff, *Cell*, 1992, **70**, 31–46.
10 R. A. Weinberg, *The Biology of Cancer: Second International Student Edition*, WW Norton & Company, 2013.
11 T. A. Martin, L. Ye, A. J. Sanders, J. Lane and W. G. Jiang, *Madame Curie Bioscience Database [Internet]*, Landes Bioscience, 2013.
12 B. Desoize and J.-C. Jardillier, *Critical Reviews in Oncology/Hematology*, 2000, **36**, 193–207.
13 S. Walenta, J. Doetsch, W. Mueller-Klieser and L. A. Kunz-Schughart, *J. Histochem. Cytochem.*, 2000, **48**, 509–522.
14 J. Laurent, C. Frongia, M. Cazales, O. Mondesert, B. Ducommun and V. Lobjois, *BMC Cancer*, 2013, **13**, 73.
15 A. M. J. Valencia, P.-H. Wu, O. N. Yogurtcu, P. Rao, J. DiGiacomo, I. Godet, L. He, M.-H. Lee, D. Gilkes and S. X. Sun, *et al.*, *Oncotarget*, 2015, **6**, 43438.
16 R. Richards, D. Mason, R. Levy, R. Bearon and V. See, *bioRxiv*, 2018, 443648.

17 N. Martino, S. J. Kwok, A. C. Liapis, S. Forward, H. Jang, H.-M. Kim, S. J. Wu, J. Wu, P. H. Dannenberg and S.-J. Jang, *et al.*, *Nat. Photonics*, 2019, **13**, 720–727.

18 Y. L. Han, A. F. Pegoraro, H. Li, K. Li, Y. Yuan, G. Xu, Z. Gu, J. Sun, Y. Hao and S. K. Gupta, *et al.*, *Nat. Phys.*, 2020, **16**, 101–108.

19 A. Palamidessi, C. Malinverno, E. Frittoli, S. Corallino, E. Barbieri, S. Sigismund, G. V. Beznoussenko, E. Martini, M. Garre and I. Ferrara, *et al.*, *Nat. Mater.*, 2019, **18**, 1252–1263.

20 J. Ranft, M. Basan, J. Elgeti, J.-F. Joanny, J. Prost and F. Jülicher, *Proc. Natl. Acad. Sci. U. S. A.*, 2010, **107**, 20863–20868.

21 D. Matoz-Fernandez, K. Martens, R. Sknepnek, J. Barrat and S. Henkes, *Soft Matter*, 2017, **13**, 3205–3212.

22 D. Bi, X. Yang, M. C. Marchetti and M. L. Manning, *Phys. Rev. X*, 2016, **6**, 021011.

23 A. N. Malmi-Kakkada, X. Li, H. S. Samanta, S. Sinha and D. Thirumalai, *Phys. Rev. X*, 2018, **8**, 021025.

24 H. S. Samanta and D. Thirumalai, *Phys. Rev. E*, 2019, **99**, 032401.

25 B. I. Shraiman, *Proc. Natl. Acad. Sci. U. S. A.*, 2005, **102**, 3318–3323.

26 K. Alessandri, B. R. Sarangi, V. V. Gurchenkov, B. Sinha, T. R. Kießling, L. Fetler, F. Rico, S. Scheuring, C. Lamaze and A. Simon, *et al.*, *Proc. Natl. Acad. Sci. U. S. A.*, 2013, **110**, 14843–14848.

27 A. D. Conger and M. C. Ziskin, *Cancer Res.*, 1983, **43**, 556–560.

28 A. Puliafito, L. Hufnagel, P. Neveu, S. Streichan, A. Sigal, D. K. Fygenson and B. I. Shraiman, *Proc. Natl. Acad. Sci. U. S. A.*, 2012, **109**, 739–744.

29 T. R. Kirkpatrick and D. Thirumalai, *Phys. Rev. A: At., Mol., Opt. Phys.*, 1988, **37**, 4439.

30 V. Almendro, A. Marusyk and K. Polyak, *Annu. Rev. Pathol.: Mech. Dis.*, 2013, **8**, 277–302.

31 T. Kirkpatrick and D. Thirumalai, *Rev. Mod. Phys.*, 2015, **87**, 183.

32 X. Li and D. Thirumalai, *J. R. Soc., Interface*, 2019, **16**, 20180820.

33 D. Drasdo and S. Höhme, *Phys. Biol.*, 2005, **2**, 133.

34 G. Schaller and M. Meyer-Hermann, *Phys. Rev. E: Stat., Nonlinear, Soft Matter Phys.*, 2005, **71**, 051910.

35 A. Malmi-Kakkada, X. Li, S. Sinha and D. Thirumalai, arXiv preprint arXiv:1906.11292, 2019.

36 A. Giri, S. Bajpai, N. Trenton, H. Jayatilaka, G. D. Longmore and D. Wirtz, *FASEB J.*, 2013, **27**, 4089–4099.

37 R. Metzler, J.-H. Jeon, A. G. Cherstvy and E. Barkai, *Phys. Chem. Chem. Phys.*, 2014, **16**, 24128–24164.

38 F. Pampaloni, N. Ansari and E. H. Stelzer, *Cell Tissue Res.*, 2013, **352**, 161–177.

39 J.-P. Hansen and I. R. McDonald, *Theory of simple liquids*, Elsevier, 1990.

40 J.-L. Barrat, J.-N. Roux and J.-P. Hansen, *Chem. Phys.*, 1990, **149**, 197–208.

41 D. Thirumalai and R. D. Mountain, *Phys. Rev. E: Stat., Nonlinear, Soft Matter Phys.*, 1993, **47**, 479.

42 L. Berthier, G. Biroli, J.-P. Bouchaud, L. Cipelletti and W. van Saarloos, *Dynamical heterogeneities in glasses, colloids, and granular media*, OUP, Oxford, 2011, vol. 150.

43 H. Kang, T. Kirkpatrick and D. Thirumalai, *Phys. Rev. E: Stat., Nonlinear, Soft Matter Phys.*, 2013, **88**, 042308.

44 A. R. Abate and D. Durian, *Phys. Rev. E: Stat., Nonlinear, Soft Matter Phys.*, 2007, **76**, 021306.

45 C. Donati, S. Franz, S. C. Glotzer and G. Parisi, *J. Non-Cryst. Solids*, 2002, **307**, 215–224.

46 J. d'Alessandro, A. P. Solon, Y. Hayakawa, C. Anjard, F. Detcheverry, J.-P. Rieu and C. Rivière, *Nat. Phys.*, 2017, **13**, 999.

47 D. Thirumalai, R. D. Mountain and T. R. Kirkpatrick, *Phys. Rev. A: At., Mol., Opt. Phys.*, 1989, **39**, 3563–3574.

48 A. Doostmohammadi, S. P. Thampi, T. B. Saw, C. T. Lim, B. Ladoux and J. M. Yeomans, *Soft Matter*, 2015, **11**, 7328–7336.